



# High $B_s$ Fe-based nanocrystalline alloy with high impurity tolerance

Lei Xie<sup>1,2</sup>, Tao Liu<sup>2,3</sup>, Aina He<sup>2,3,\*</sup>, Qiang Li<sup>1,\*</sup>, Zhikai Gao<sup>2</sup>, Anding Wang<sup>2,3,4,\*</sup> , Chuntao Chang<sup>2,3</sup>, Xinmin Wang<sup>2,3</sup>, and C. T. Liu<sup>4</sup>

<sup>1</sup> School of Physics Science and Technology, Xinjiang University, Ürümqi 830046, Xinjiang, China

<sup>2</sup> Key Laboratory of Magnetic Materials and Devices, Ningbo Institute of Materials Technology and Engineering, Chinese Academy of Sciences, Ningbo 315201, Zhejiang, China

<sup>3</sup> Zhejiang Province Key Laboratory of Magnetic Materials and Application Technology, Ningbo Institute of Materials Technology and Engineering, Chinese Academy of Sciences, Ningbo 315201, China

<sup>4</sup> Center for Advanced Structural Materials, Department of Mechanical and Biomedical Engineering, College of Science and Engineering, City University of Hong Kong, Kowloon, Hong Kong, China

Received: 24 May 2017

Accepted: 7 September 2017

© Springer Science+Business Media, LLC 2017

## ABSTRACT

High  $B_s$  Fe<sub>82.5</sub>Si<sub>3</sub>B<sub>13</sub>P<sub>0.5</sub>C<sub>0.2</sub>Cu<sub>0.8</sub> alloys with high impurity tolerance were successfully developed and prepared into ribbons with fully amorphous and uniform nanocrystalline microstructure. By comparing samples made with industrial grade and pure raw materials, it is found that the impurities in the commonly used industrial grade raw materials mainly affect the amorphous forming ability and amorphous structure of the as-spun ribbons. The effects of impurities on crystallization behaviors and magnetic properties can be inhibited in the amorphous ribbon production process for the alloys with a high impurity tolerance. The Fe<sub>82.5</sub>Si<sub>3</sub>B<sub>13</sub>P<sub>0.5</sub>C<sub>0.2</sub>Cu<sub>0.8</sub> nanocrystalline alloy ribbons prepared with industrial grade raw materials exhibit excellent magnetic properties, containing high  $B_s$  over 1.79 T, low  $H_c$  of 9.5 A/m and maximum permeability ( $\mu_m$ ) of  $4 \times 10^4$ , which are similar to the samples made with pure raw materials with unacceptable high cost. Combining the low cost of raw materials, good manufacturability and excellent magnetic properties, the present Fe<sub>82.5</sub>Si<sub>3</sub>B<sub>13</sub>P<sub>0.5</sub>C<sub>0.2</sub>Cu<sub>0.8</sub> alloy will become a promising candidate for mass production and also provide a good reference for future development of high  $B_s$  nanocrystalline alloys.

## Introduction

Soft magnetic materials, which play a key role in both power generation–conversion and electronics fields, have aroused enormous attentions and investigations

for continuously improving their magnetic properties, containing higher saturation magnetization ( $B_s$ ), lower coercivity ( $H_c$ ), higher permeability ( $\mu$ ) and lower core losses [1, 2], to realize the miniaturization and higher efficiency of electrical devices. After a

Address correspondence to E-mail: hean@nimte.ac.cn; qli@xju.edu.cn; anding@nimte.ac.cn

century development, various soft magnetic materials have been developed and used in different fields according to their unique performance [3]. Besides their diversified magnetic properties, the price is also an important factor for composition design and applications of soft magnetic materials. Since the cost of raw materials for commercialization of amorphous and nanocrystalline alloys greatly depends on compositions [4], a systematically statistical study on the  $B_s$  and price of the commonly used soft magnetic materials is conducted, as shown in Fig. 1. It is obvious that the Si-steel exhibits the highest  $B_s$  and lowest price, which explains their wide application in transformers and motors, etc. [5]. This also presses us to decrease the price and increase the  $B_s$  of the new generation materials with superior soft magnetic properties, especially for amorphous and nanocrystalline alloys. For the amorphous systems, the commercial high  $B_s$  FeSiB and FeSiBC alloys have been proved to exhibit limited space for the improvement of  $B_s$  and  $\mu_{er}$ , and other systems with high content of metallic amorphous forming elements suffer the low  $B_s$  and high price. By comprehensive consideration of the  $B_s$ ,  $\mu$  and price, it is clear that the high  $B_s$  nanocrystalline alloys (HBNAs) without non-magnetic metallic elements that exhibit high  $B_s$  comparable to that of Si-steel, in addition, the much higher  $\mu$  and lower price, are the most attractive and promising ones for applications in the power fields, which are occupied by high energy cost Si-steel now [6, 7].

Since the first HBNA was developed in 2007 by Ohta et al., a series of HBNAs such as FeBCu [17], FeSiBCu [18], FeSiBPCu [19], FeSiBPCCu [20] and FeSiBCCu [21] were successfully developed, which were characterized by high Fe content, absence of large atomic radius metallic elements such as Nb and Mo, and extremely high  $B_s$  even above 1.80 T. However, the following investigations explored the key obstacles in harsh ribbon production and annealing processes, which originated from the poor amorphous forming ability (AFA), low thermal stability and fast diffusion nature [22, 23]. Compared with the conventional Finemet [24], Nanoperm [25] and Hitperm [11] alloys, these alloys exhibit much higher sensitivity of magnetic properties and nanocrystalline structure on as-spun parameters and annealing process, which underlying mechanisms are still not absolutely clear, different from the unveiled crystallization mechanism and implications for properties of Finemet-type alloys [26]. In addition, these unveiled questions become more spiny and complicated when industrial grade raw materials are adopted, which will inevitably introduce the impurity effects. Most of the documented alloys were prepared with pure raw materials (PRMs), which price is about 300 times than that of industrial grade raw materials (IRMs), as highlighted in Fig. 1. Few alloys were designed or investigated from the aspects of IRMs and the impurity effects on performance. Consequently, the development of HBNAs based on IRMs and

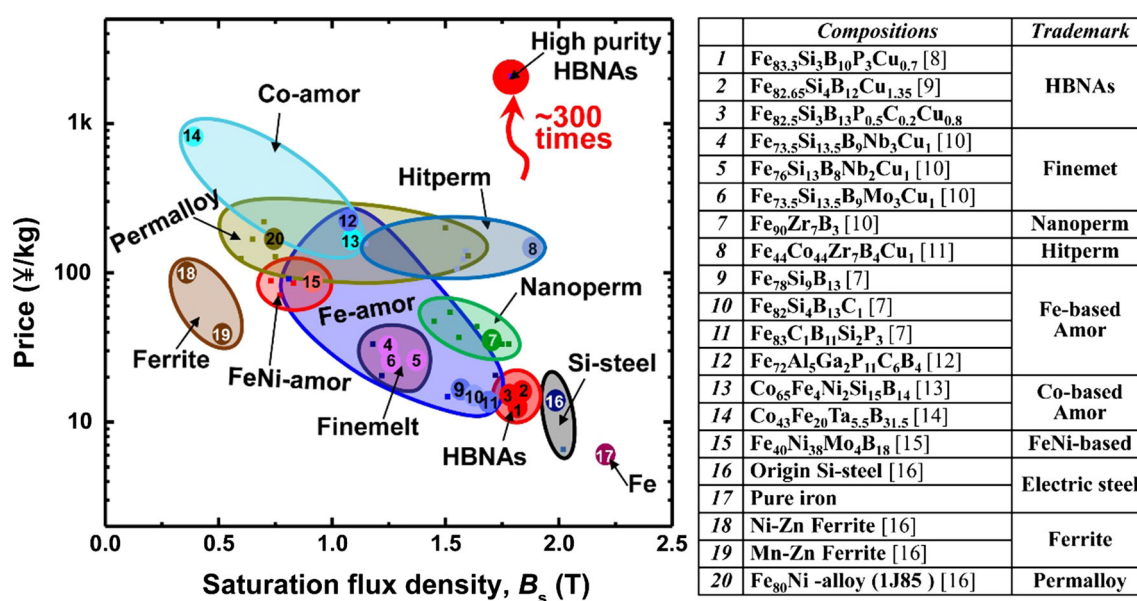


Figure 1 The  $B_s$  and price of the commonly used soft magnetic materials.

exploration of the impurity effects on magnetic properties, nanocrystalline structure as well as the microstructure evolution during annealing process are very important to the applications and of great scientific significance. Since HBNA are too impurity sensitive and hardly made with industrial grade materials, the effect of purity is currently the primary concern.

In this study, the  $Fe_{82.5}Si_3B_{13}P_{0.5}C_{0.2}Cu_{0.8}$  nanocrystalline alloy with high impurity tolerance for IRMs was successfully developed, from the comprehensive considerations of the constituent elements on the AFA, magnetic properties and manufacturability. Samples prepared with PRMs and IRMs are all comparatively investigated to explore the effects of purity on magnetic properties and crystallization behaviors. Microstructure and magnetic domains of the nanocrystalline alloy ribbons prepared with IRMs were investigated in detail, to reveal the correlation between magnetic properties and microstructure. These results will be of great significance for the future development and applications of HBNA.

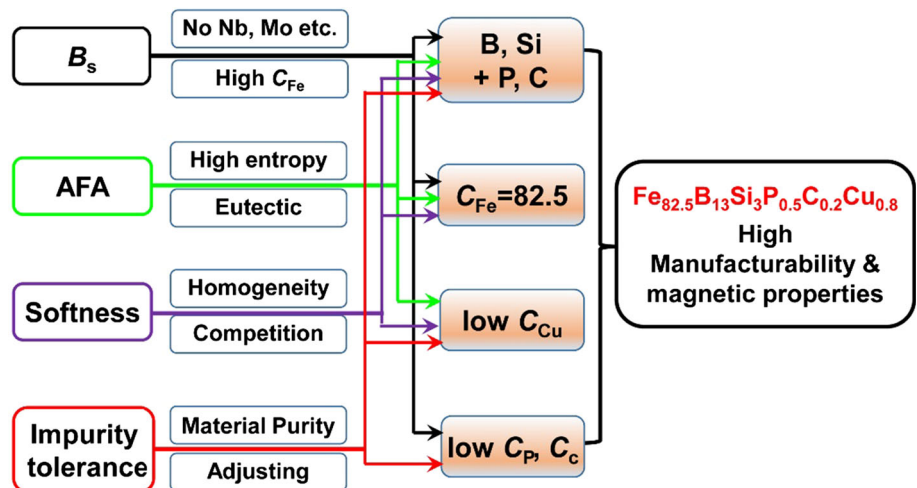
### Composition design methods

According to the results of statistical analysis of HBNA and our long-term investigation, we propose a composition design method for the HBNA as illustrated in Fig. 2. In consideration of the  $B_s$ , AFA, softness and impurity tolerance for the HBNA, the content of the three requisite kinds of elements, i.e., ferromagnetic element, metalloid element and nucleation motivating element, were determined. The

composition design method was drawn from the following aspects:

1. As for achieving high  $B_s$  of these alloys, the transition metal elements (Nb, Mo, etc.) with large atomic radius are always excluded and relatively high Fe content ( $C_{Fe}$ ) was chosen. Metalloid elements such as Si, B, P and C with low atomic number and atom radius are selected, in order to enhance the coupling interaction between Fe atoms [7]. The contents of P and C ( $C_P$  and  $C_C$ ), which are reported to reduce the  $B_s$ , are restricted to be low values.
2. As proposed before, the eutectic points of Fe and B, P and C are all closed to 83 at.% and the Si is mutually soluble in Fe in this range. The composition with Fe content around 83 at.% and 17 at.% of Si, B, P and C in total is considered to be closed to the eutectic point and prone to exhibit high AFA. Meanwhile, the multicomponent system means high entropy, which is also contributed to the high AFA [27]. Since the nucleation motivating element Cu with high content may decrease the AFA of Fe-based alloys, a low Cu content of 0.8 at.% was chosen [17, 19, 21].
3. We know that the soft magnetic properties are greatly dependent on the nanocrystalline microstructure containing grain size, grain density and distribution uniformity, which are determined by the homogeneity of the as-spun ribbon and competition effect in nanocrystallization process. Cu with proper content can stimulate the nucleation and avoid large primary precipitation, which is good for the formation of uniform

**Figure 2** Illustration of the composition design method of high  $B_s$  nanocrystalline alloys.



microstructure. The relatively high Fe content is conducive to form high density of  $\alpha$ -Fe grains [28] and enhance the competing effect during grain growth. The metalloid elements P and C are also important for refining the grain size and improving the stability of the residual amorphous phase [7, 29].

- As declared above, the impurity tolerance is a main obstacle for the application of HBNA and also is the most concerned factor in this study. Since the preparation process of pre-alloy FeP and FeC is still needed to be improved as FeB alloy used in FeSiB and FeSiBNbCu alloys, the addition of P and C elements will introduce many impurities. Thus, the addition of P and C should be controlled, but is still required for improving the AFA and manufacturability, especially for refining the grains [7].

Based on the upper analysis,  $\text{Fe}_{82.5}\text{Si}_3\text{B}_{13}\text{P}_{0.5}\text{C}_{0.2}\text{Cu}_{0.8}$  nanocrystalline alloy was designed to study, which is promising to exhibit high AFA, impurity tolerance and manufacturability, together with excellent magnetic properties.

## Experimental procedures

Multicomponent alloy with nominal atomic composition of  $\text{Fe}_{82.5}\text{Si}_3\text{B}_{13}\text{P}_{0.5}\text{C}_{0.2}\text{Cu}_{0.8}$  was designed. The master alloys were prepared with pure raw materials (PRMs) of Fe (99.99 wt.%), Si (99.99 wt.%), B (99.9 wt.%), Cu (99.99 wt.%), pre-alloy of Fe<sub>3</sub>P, Fe–3.6% C and industrial grade raw materials (IRMs) of Fe (99 wt.%), Si (99.85 wt.%), Cu (99.95 wt.%), pre-alloy of Fe–23%P, Fe–23%C and Fe–18%B, respectively. Then, these alloys were melt by induction melting under Ar atmosphere after high vacuum of about  $1 \times 10^{-2}$  Pa. Ribbons with width of about 0.70 mm and thickness of about 24  $\mu\text{m}$  were prepared through single-roller melt-spinning method. The thermal properties were investigated by differential scanning calorimetry (DSC, NETZSCH 404C) at a heating rate of 40  $^{\circ}\text{C}/\text{min}$ . Isothermal annealing was carried out under a certain temperature for 3 min followed by water quenching. The microstructures of as-quenched and annealed ribbons were investigated by X-ray diffraction (XRD, Bruker D8 Advance) with Cu-K $\alpha$  radiation and high-resolution transmission electron microscopy (TEM, TECNAI F20). The magnetic

domains were observed on the air-bare surface by Kerr microscopy under different magnetic fields, without further sample preparation such as polishing or coating. The mass of the samples was measured by using an electronic balance with high accuracy of  $\pm 0.00001$  g (Mettler XS105DU), and the density of the samples was measured by the Archimedeian method. All the mass and density values were averaged by multiple tests in order to ensure the reproducibility. The magnetic properties including saturation magnetization ( $B_s$ ), coercivity ( $H_c$ ) and effective permeability ( $\mu_e$ ) were measured with vibrating sample magnetometer (VSM, Lake Shore 7410) under the maximum applied field of 800 kA/m (commonly used value), B-H loop tracer (EXPH-100) under the maximum applied field of 800 A/m and impedance analyzer (Agilent 4294 A) under the applied field from 1 to 100 A/m, respectively. All the measurements were performed at room temperature.

## Results and discussion

The melt-spun  $\text{Fe}_{82.5}\text{Si}_3\text{B}_{13}\text{P}_{0.5}\text{C}_{0.2}\text{Cu}_{0.8}$  alloy ribbons prepared with the PRMs and IRMs at different wheel speeds ( $v$ ) exhibit really good surface quality and bending ductility. The amorphous state of these ribbons with different thicknesses ( $D$ ) was then identified by XRD from the free side, as shown in Fig. 3. The ribbons prepared at even low  $v$  of 20 m/s with PRMs exhibit fully amorphous structure characterized with only a halo peak, indicating high AFA of this alloy. For the alloy made with IRMs, amorphous ribbon samples can be prepared only at a relatively

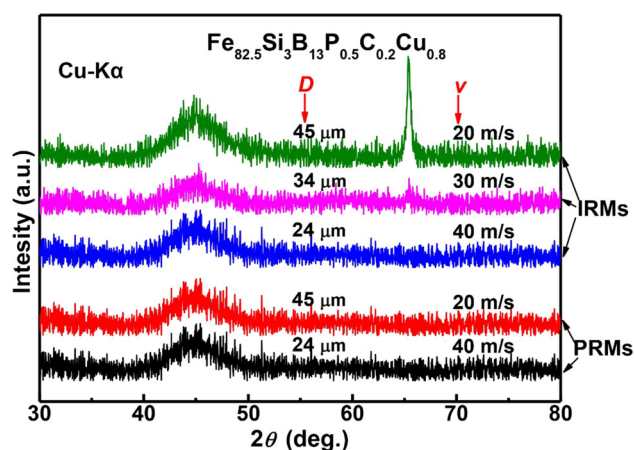


**Figure 3** XRD patterns of the melt-spun  $\text{Fe}_{82.5}\text{Si}_3\text{B}_{13}\text{P}_{0.5}\text{C}_{0.2}\text{Cu}_{0.8}$  ribbons prepared with IRMs and PRMs at different  $v$ .

higher  $v$  of 30–40 m/s, which is acceptable for the industrial production. However, the sharp crystallization peak at  $2\theta = 65^\circ$  in XRD spectrum of the ribbon is prepared with IRMs at  $v = 20$  m/s, and the sharp crystallization peak at  $2\theta = 65^\circ$  illustrates the crystallization, indicating the tiny decrease in AFA caused by the purities in the IRMs. Therefore, we can conclude that the present  $\text{Fe}_{82.5}\text{Si}_3\text{B}_{13}\text{P}_{0.5}\text{C}_{0.2}\text{Cu}_{0.8}$  alloy exhibits a high AFA and a high impurity tolerance.

The thermal performance of the melt-spun  $\text{Fe}_{82.5}\text{Si}_3\text{B}_{13}\text{P}_{0.5}\text{C}_{0.2}\text{Cu}_{0.8}$  alloy ribbons was investigated by DSC, as shown in Fig. 4. The DSC curves of the melt-spun ribbons prepared with PRMs and IRMs both exhibit two distinct exothermic peaks with the onset temperatures marked as  $T_{x1}$  and  $T_{x2}$ . As reported [15], the first and second crystallization peaks are corresponding to the precipitations of  $\alpha$ -Fe phase and compounds such as boride and phosphide, respectively [30, 31]. The ribbons prepared with IRMs and PRMs exhibit wide temperature intervals  $\Delta T_x$  ( $\Delta T_x = T_{x2} - T_{x1}$ ) of 107 and 109 K, respectively, which is favorable for controllable precipitation of  $\alpha$ -Fe during the annealing process [32, 33] and achievement of excellent magnetic properties. In addition, the DSC curve of the ribbons prepared with IRMs at  $v = 30$  m/s is almost overlapping with the ribbons with IRMs at  $v = 40$  m/s as shown in Fig. 4, indicating the negligible effect of impurities on thermal performance. We can hence deduce that the tiny difference of the  $\Delta T_x$  between the ribbon prepared

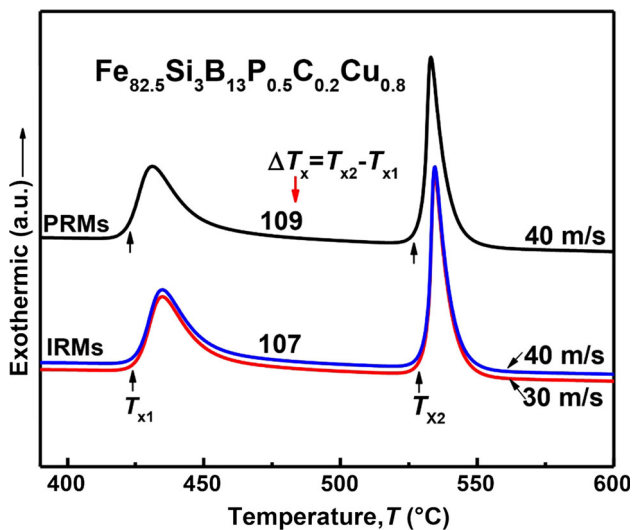


**Figure 4** DSC traces of the melt-spun  $\text{Fe}_{82.5}\text{Si}_3\text{B}_{13}\text{P}_{0.5}\text{C}_{0.2}\text{Cu}_{0.8}$  ribbons prepared with IRMs and PRMs.

with PRMs and one prepared with IRMs should originate from the composition deviation induced by alloying.

The change of coercivity ( $H_c$ ) of the present ribbon samples as a function of annealing temperature ( $T_A$ ) is shown in Fig. 5. Generally, the annealing process of the nanocrystalline alloys can be divided into three stages: stress release, nanocrystallization and precipitation of the second phases. During the stress release stage, the defects like free volume can be eliminated, resulting in a more uniform microstructure and thus the decrease in  $H_c$ . With the increase in  $T_A$ , the  $H_c$  increases sharply at the relatively low temperature due to precipitation of the coarse grains with low crystallinity [27, 34]. While during the optimal annealing window, high density of  $\alpha$ -Fe grains precipitates simultaneously and grows up competitively, resulting in a uniform microstructure with fine grains, and thus a minimum value of  $H_c$ . When  $T_A$  is higher than the optimal window, the precipitation of coarse grains and other phases causes a sharp deterioration in  $H_c$ . It is obvious that the changes of  $H_c$  as a function of  $T_A$  for the  $\text{Fe}_{82.5}\text{Si}_3\text{B}_{13}\text{P}_{0.5}\text{C}_{0.2}\text{Cu}_{0.8}$  alloy ribbons prepared with PRMs and IRMs exhibit a similar tendency, the optimal  $T_A$  for the two alloys is both 520 °C, and the obtained  $H_c$  for the ribbons prepared with IRMs is 9.5 A/m, which is even little lower than that (10.8 A/m) of the ribbons prepared with PRMs. It is hence concluded that the impurities have a negligible effect on the magnetic properties, implying the high impurity tolerance of the present alloys.

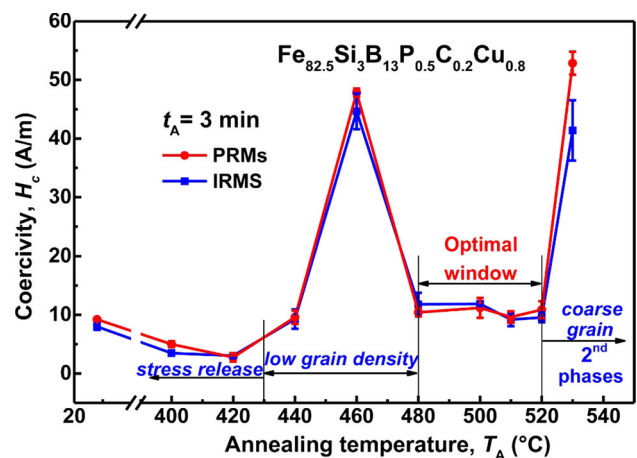


**Figure 5**  $H_c$  of the  $\text{Fe}_{82.5}\text{Si}_3\text{B}_{13}\text{P}_{0.5}\text{C}_{0.2}\text{Cu}_{0.8}$  alloy ribbons dependence on  $T_A$  after annealing for 3 min.

According to the investigation in Fig. 5, we determined that the optimum  $T_A$  is 520 °C. The hysteresis loops of the annealed alloy ribbons were then measured with VSM, as shown in Fig. 6. As enlarged in the insert (a), we can see that the  $B_s$  of the ribbons prepared with IRMs and PRMs is the almost same value of 1.79 T. Insert (b) enlarged  $B$ - $H$  loops of these alloys by DC magnetic field amplitude. It is interested that the  $H_c$  of the samples prepared with IRMs is slightly lower, indicating the improvement of performance of the designed  $\text{Fe}_{82.5}\text{Si}_3\text{B}_{13}\text{P}_{0.5}\text{C}_{0.2}\text{Cu}_{0.8}$  alloy prepared with IRMs [35]. For simplify, the following characterizations of  $\mu_e$  and microstructure were only carried out for the samples prepared with IRMs.

For the consideration of the applications of the designed  $\text{Fe}_{82.5}\text{Si}_3\text{B}_{13}\text{P}_{0.5}\text{C}_{0.2}\text{Cu}_{0.8}$  nanocrystalline alloy, the relative permeability ( $\mu$ ) of the annealed ribbons under different AC magnetic field amplitude ( $H_m$ ) and frequency is an important parameter [36, 37]. The frequency dependence of  $\mu$  at the selected  $H_m$  is shown in Fig. 7. With the increase in  $H_m$ , the  $\mu$  increases from  $9.0 \times 10^3$  ( $H_m = 1$  A/m) to  $4 \times 10^4$  ( $H_m = 30$  A/m) and then decreases to  $1.7 \times 10^4$  ( $H_m = 100$  A/m) again at 400 Hz. The maximum value of the permeability occurs under magnetic field with amplitude  $H_m = 30$  A/m, and it can be considered as the  $\mu_m$ . It is interesting that the alloy exhibits excellent frequency properties at a low  $H_m$  of 1 A/m and a high  $H_m$  of 50–100 A/m.

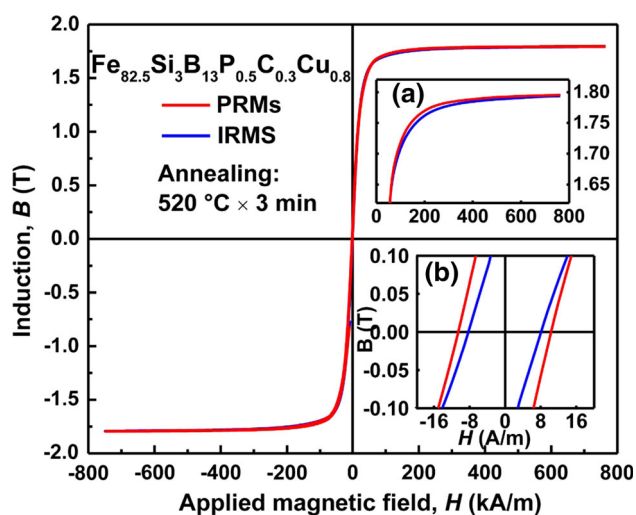


**Figure 6** Hysteresis loops of the  $\text{Fe}_{82.5}\text{Si}_3\text{B}_{13}\text{P}_{0.5}\text{C}_{0.2}\text{Cu}_{0.8}$  alloy ribbons after annealing at optimum conditions; inset (a) partial enlarged graph of the hysteresis loops; inset (b) enlarged  $B$ - $H$  loops of these alloys.

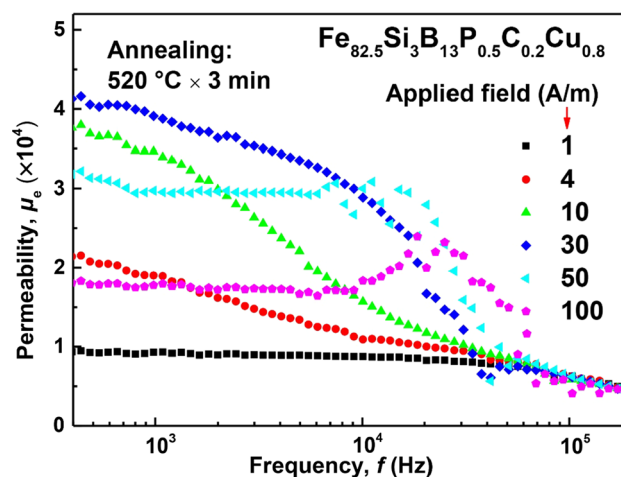


**Figure 7** The changes of  $\mu$  as a function of frequency at selected AC magnetic field amplitude from 400 Hz to 1 MHz for the  $\text{Fe}_{82.5}\text{Si}_3\text{B}_{13}\text{P}_{0.5}\text{C}_{0.2}\text{Cu}_{0.8}$  alloy ribbons prepared with IRMs.

The  $\mu$  does not decrease distinctly in a wide range below cutoff frequency of about 25 kHz. The high  $\mu$  over  $9.0 \times 10^3$  together with excellent frequency properties will make the  $\text{Fe}_{82.5}\text{Si}_3\text{B}_{13}\text{P}_{0.5}\text{C}_{0.2}\text{Cu}_{0.8}$  nanocrystalline alloy prospective candidates for various electric devices.

The thermal parameters and magnetic properties of the present alloy together with other typical compositions as contrastively are summarized in Table 1. These typical compositions are all prepared with PRMs, except for the present alloy which was successfully prepared with IRMs. The present  $\text{Fe}_{82.5}\text{Si}_3\text{B}_{13}\text{P}_{0.5}\text{C}_{0.2}\text{Cu}_{0.8}$  alloy ribbons exhibit a wide  $\Delta T_x$  around 108 °C, high  $B_s$  of 1.79 T and low  $H_c$  around 10.0 A/m, which is better than that of the  $\text{Fe}(\text{Si})\text{BCCu}$  [21],  $\text{Fe}(\text{Si})\text{PCu}$  [38] and  $\text{FePCCu}$  [39] after conversational annealing. We should also note that the  $\text{FeSiBCu}$  [18] and  $\text{FeSiBPCu}$  [19] alloy exhibit larger  $\Delta T_x$  and better magnetic performance compared with the present alloy; however, the excellent magnetic properties were obtained for these alloys through flash annealing, which is difficult for the mass production. The present alloy exhibits high impurity tolerance, which can be prepared with IRMs in a low price, and also exhibits excellent magnetic properties after conversational annealing, which is promising to be widely applied in electronics fields.

To reveal the reasons for the excellent magnetic properties of the present nanocrystalline alloy, the microstructure of the ribbons prepared with IRMs during the annealing process was investigated in detail. The XRD patterns of the  $\text{Fe}_{82.5}\text{Si}_3\text{B}_{13}\text{P}_{0.5}\text{C}_{0.2}\text{Cu}_{0.8}$

**Table 1**  $\Delta T_x$ , annealing process and magnetic properties of the present  $\text{Fe}_{82.5}\text{Si}_3\text{B}_{13}\text{P}_{0.5}\text{C}_{0.2}\text{Cu}_{0.8}$  alloys (prepared with IRMs and PRMs) compared with other typical high  $B_s$  nanocrystalline alloys after annealing under optimal conditions

| System                       | Raw materials | $\Delta T_x$ (°C) | Annealing process        | $B_s$ (T)       | $H_c$ (A/m) |         |
|------------------------------|---------------|-------------------|--------------------------|-----------------|-------------|---------|
| $\text{FeSiBPCCu}$ (present) | Industrial    | 107               | Conversational annealing | 1.79            | 9.5         |         |
| $\text{FeSiBPCCu}$ (present) | Pure          | 109               |                          | 1.79            | 10.8        |         |
| $\text{FeSiBPCCu}$ [20]      |               | 112–145           |                          | 1.78–1.83       | 4.5–750     |         |
| $\text{FeSiPC(Cu)}$ [40]     |               | 100–110           |                          | 1.55–1.68       | 14.2–26.7   |         |
| $\text{Fe(Si)BCCu}$ [21]     |               | 84–106            |                          | 1.72–1.81       | 5–8         |         |
| $\text{Fe(Si)PCu}$ [38]      |               | 46–88             |                          | 1.58–1.65       | 3.3–15      |         |
| $\text{FeSiBPCu}$ [19]       |               | 136–154           |                          | Flash annealing | 1.74–1.82   | 6.5–7.2 |
| $\text{Fe(Si)BCu}$ [17, 18]  |               | 135–175           |                          |                 | 1.71–1.84   | 6.5–190 |

alloy ribbons after annealing at different  $T_A$  for 3 min are shown in Fig. 8, together with the calculated grain size according to Scherrer equation [41]. The sharp crystalline peaks, which can be identified as  $\alpha$ -Fe, can be easily observed for the annealed ribbons. With the increase in  $T_A$ , the grain size decreases to a minimum at 520 °C and then increases again. The changes of the grain size with  $T_A$  are a good explanation for the change of the  $H_c$  with  $T_A$  as shown in Fig. 5, since the  $H_c$  is greatly dependent on the microstructure.

In order to obtain more convincing and detailed microstructure, the TEM characterizations of the sample after annealing under optimal conditions were carried out. The bright-field image, selected area electron diffraction (SAED) patterns and grain size distribution for the annealed  $\text{Fe}_{82.5}\text{Si}_3\text{B}_{13}\text{P}_{0.5}\text{C}_{0.2}\text{Cu}_{0.8}$  alloy ribbons are shown in Fig. 9. The grains, which can be identified as  $\alpha$ -Fe from the SAED

patterns, distribute evenly on amorphous matrix. As exhibited in Fig. 9c, the average grain size is 16.3 nm, which coincides with the result calculated from Scherrer equation [41] as shown in Fig. 8. The uniform microstructure with the fine grains is the main reason for the excellent magnetic properties of the sample annealed at 520 °C.

For further understanding the excellent magnetic properties of the present alloy, magnetic domains under different magnetic field of the  $\text{Fe}_{82.5}\text{Si}_3\text{B}_{13}\text{P}_{0.5}\text{C}_{0.2}\text{Cu}_{0.8}$  ribbon sample after annealing at 520 °C for 3 min were studied with magneto-optical Kerr microscopy. The magnetic domains taken from the position together with the sensitive direction and ribbon axis are illustrated in Fig. 10a. According to the B-H loops in Fig. 10b, the magnetic domains were observed at the selected field as shown in Fig. 10c–h. The wide stripe domains with preferred orientation nearly perpendicular to the ribbon axis can be easily observed, and the domain walls are not smooth. This phenomenon may be attributed to the edge effect, which always accompanies stress increase, changing of inner stress direction and surface quality [42]. To further investigate the magnetization process, the domains were observed by applying an increasing external magnetic field ( $H$ ) with direction along the ribbon axis. As shown in Fig. 8c–h, with the increase in  $H$ , the domain walls gradually become smooth and move to the right. The domain walls can be easily moved in a small  $H$ , demonstrating the excellent soft magnetic property of this alloy. Magnetic saturation is not achieved until the magnetic field strength reaches 240 A/m.

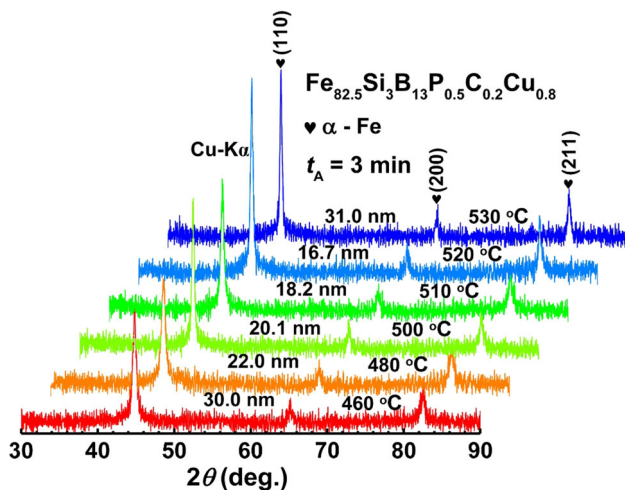


**Figure 8** XRD patterns of the  $\text{Fe}_{82.5}\text{Si}_3\text{B}_{13}\text{P}_{0.5}\text{C}_{0.2}\text{Cu}_{0.8}$  alloy ribbons prepared with IRMs after annealing at different  $T_A$  for 3 min.

**Figure 9** TEM bright-field images, selected area electron diffraction (SAED) patterns and grain size distribution for the  $\text{Fe}_{82.5}\text{Si}_3\text{B}_{13}\text{P}_{0.5}\text{C}_{0.2}\text{Cu}_{0.8}$  alloy ribbons prepared with IRMs after annealing at  $520\text{ }^\circ\text{C}$  for 3 min.

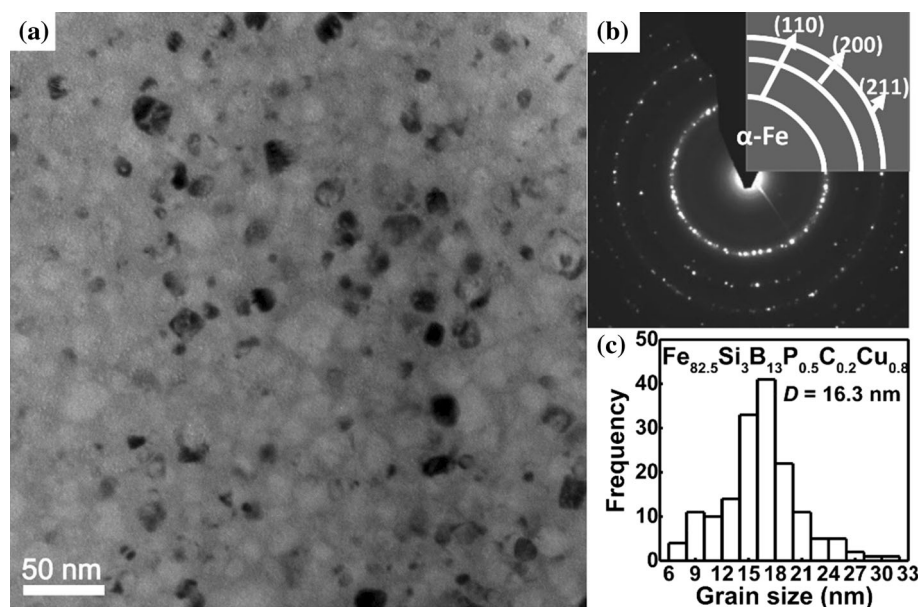
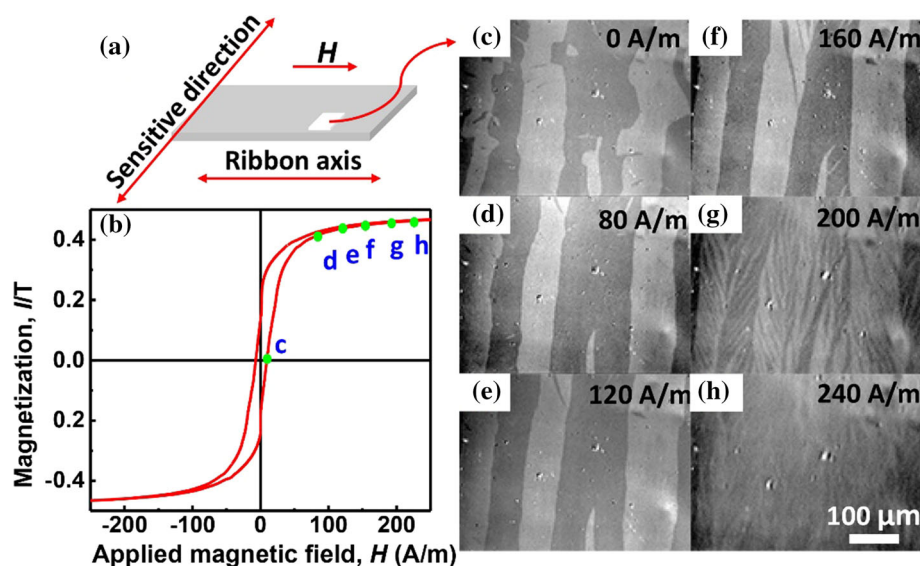


**Figure 10** Magnetic domains of the  $\text{Fe}_{82.5}\text{Si}_3\text{B}_{13}\text{P}_{0.5}\text{C}_{0.2}\text{Cu}_{0.8}$  alloy ribbons prepared with IRMs after annealing at  $520\text{ }^\circ\text{C}$  for 3 min, **a** schematic diagram of strip position and applied field; **b** B-H loops of the annealed ribbons; **c-h** magnetic domains obtained under the field of 0, 80, 120, 160, 200 and 240 A/m, respectively.



## Conclusions

In this work, high  $B_s$   $\text{Fe}_{82.5}\text{Si}_3\text{B}_{13}\text{P}_{0.5}\text{C}_{0.2}\text{Cu}_{0.8}$  nanocrystalline alloy was designed and readily prepared into high-quality ribbons with PRMs and IRMs. The magnetic properties, microstructure and magnetic domains were investigated in detail. The obtained results are as follows:

1. The designed  $\text{Fe}_{82.5}\text{Si}_3\text{B}_{13}\text{P}_{0.5}\text{C}_{0.2}\text{Cu}_{0.8}$  alloy exhibits high AFA, which can be prepared into the fully amorphous ribbons with a critical thickness of 45 and  $34\text{ }\mu\text{m}$  with PRMs and IRMs, respectively. The purities in the commonly used

industrial grade raw materials mainly affect the AFA and amorphicity of the as-spun ribbons.

2. The effects of impurities on thermal performance and magnetic properties of amorphous precursor ribbons can be negligible. The ribbons prepared with PRMs and IRMs both exhibit a wide  $\Delta T_x$  over  $100\text{ }^\circ\text{C}$ , low  $H_c$  of about  $10\text{ A/m}$  and high  $B_s$  over  $1.79\text{ T}$ .
3. The ribbons prepared with IRMs after annealing also exhibit good frequency properties, which is attributed to the uniform microstructure with a small grain size of  $16.3\text{ nm}$  and the easily moved magnetic domains.

## Acknowledgements

This work was mainly supported by the National Natural Science Foundation of China (Grant Nos. 51601206, 51671206), Ningbo International Cooperation Projects (Grant No. 2015D10022), the National Key Research and Development Program of China (Grant No. 2016YFB0300501) and Ningbo Major Project for Science and Technology (Grant No. 2014 01B1003003), and. A. D Wang, C.T. Chang and C.T. Liu were also supported by General Research Fund of Hong Kong under the grant number of CityU 102013.

## Compliance with ethical standards

**Conflict of interest** The authors declare that they have no conflict of interest.

## References

- [1] Gutfleisch O, Willard MA, Bruck E, Chen CH, Sankar SG, Liu JP (2011) Magnetic materials and devices for the 21st century: stronger, lighter, and more energy efficient. *Adv Mater* 23:821–842
- [2] Herzer G (2013) Modern soft magnets: amorphous and nanocrystalline materials. *Acta Mater* 61:718–734
- [3] Wang AD, Zhao CL, He A, Men H, Chang CT, Wang XM (2016) Composition design of high Bs Fe-based amorphous alloys with good amorphous-forming ability. *J. Alloys Compd.* 656:729–734
- [4] Kurniawan M, Keylin V, McHenry ME (2015) Effect of alloy substituents on soft magnetic properties and economics of Fe-based and co-based alloys. *J Mater Res* 30:2231–2237
- [5] McHenry ME, Laughlin DE (2000) Nano-scale materials development for future magnetic applications. *Acta Mater* 48:223–238
- [6] Ogawa Y, Naoe M, Yoshizawa Y, Hasegawa R (2006) Magnetic properties of high Fe-based amorphous material. *J Magn Magn Mater* 304:675–677
- [7] Wang AD, Zhao CL, Men H et al (2015) Fe-based amorphous alloys for wide ribbon production with high B-s and outstanding amorphous forming ability. *J Alloys Compd* 630:209–213
- [8] Dan Z, Qin F, Zhang Y, Makino A, Chang H, Hara N (2016) Mechanism of active dissolution of nanocrystalline FeSiBPCu soft magnetic alloys. *Mater Charact* 121:9–16
- [9] Ohta M, Yoshizawa Y (2007) Magnetic properties of nanocrystalline Fe<sub>82.65</sub>Cu<sub>1.35</sub>Si<sub>6</sub>B<sub>16-x</sub> alloys (x = 0–7). *Appl Phys Lett* 91:062517-3
- [10] McHenry ME, Willard MA, Laughlin DE (1999) Amorphous and nanocrystalline materials for applications as soft magnets. *Prog Mater Sci* 44:291–443
- [11] Willard MA, Huang MQ, Laughlin DE et al (1999) Magnetic properties of HITPERM (Fe, Co)(88)Zr7B4Cu1 magnets. *J Appl Phys* 85:4421–4423
- [12] Mitrovic N, Kane S, Roth S, Kalezic-Glisovic A, Mickel C, Eckert J (2012) The precipitation of nanocrystalline structure in the joule heated Fe<sub>72</sub>Al<sub>5</sub>Ga<sub>2</sub>P<sub>11</sub>C<sub>6</sub>B<sub>4</sub> metallic glasses. *J Min Metall Sect B Metall* 48:319–324
- [13] Zhou X, Zhou H, Zhao Z, Liu R, Zhou Y (2012) A study of non-isothermal primary crystallization kinetics and soft magnetic property of Co<sub>65</sub>Fe<sub>4</sub>Ni<sub>2</sub>Si<sub>15</sub>B<sub>14</sub> amorphous alloy. *J Alloys Compd* 539:210–214
- [14] Inoue A, Shen BL, Koshiba H, Kato H, Yavari AR (2003) Cobalt-based bulk glassy alloy with ultrahigh strength and soft magnetic properties. *Nat Mater* 2:661–663
- [15] Ok HN, Morrish AH (1981) Surface crystallization and magnetic-anisotropy in amorphous Fe<sub>40</sub>Ni<sub>38</sub>Mo<sub>4</sub>B<sub>18</sub> ribbons. *J Appl Phys* 52:1835–1837
- [16] Herzer G (1997) Chapter 3 nanocrystalline soft magnetic alloys In: Buschow, K.H.J., (ed.), *Handbook of magnetic materials*, vol 10. Elsevier Science B.V., Amsterdam, The Netherlands, pp 415–462
- [8] Ohta M, Yoshizawa Y (2007) Improvement of soft magnetic properties in (Fe<sub>0.85</sub>B<sub>0.15</sub>)(100-x)Cu-x melt-spun alloys. *Mater Trans* 48:2378–2380
- [18] Ohta M, Yoshizawa Y (2011) Recent progress in high B-s Fe-based nanocrystalline soft magnetic alloys. *J Phys D Appl Phys* 44:064004
- [19] Urata A, Matsumoto H, Yoshida S, Makino A (2010) In: Nie JF, Morton A (eds) *Prism 7*, Pts 1–3 Trans Tech Publications Ltd, Durnten-Zurich
- [20] Takenaka K, Setyawan AD, Sharma P, Nishiyama N, Makino A (2016) Industrialization of nanocrystalline Fe–Si–B–P–Cu alloys for high magnetic flux density cores. *J Magn Magn Mater* 401:479–483
- [21] Fan XD, Shen BL (2015) Crystallization behavior and magnetic properties in High Fe content FeBCSiCu alloy system. *J Magn Magn Mater* 385:277–281
- [22] Ohta M, Yoshizawa Y (2009) Effect of heating rate on soft magnetic properties in nanocrystalline Fe<sub>80.5</sub>Cu<sub>1.5</sub>Si<sub>4</sub>B<sub>14</sub> and Fe<sub>82</sub>Cu<sub>1</sub>Nb<sub>1</sub>Si<sub>4</sub>B<sub>12</sub> alloys. *Appl Phys Express* 2:23005-3
- [23] Sharma P, Zhang X, Zhang Y, Makino A (2014) Influence of microstructure on soft magnetic properties of low coreloss and high B-s Fe<sub>85</sub>Si<sub>2</sub>B<sub>8</sub>P<sub>4</sub>Cu<sub>1</sub> nanocrystalline alloy. *J Appl Phys* 115:17A340–17A343

- [24] Yoshizawa Y, Oguma S, Yamauchi K (1988) New Fe-based soft magnetic-alloys composed of ultrafine grain-structure. *J Appl Phys* 64:6044–6046
- [25] Suzuki K, Kataoka N, Inoue A, Makino A, Masumoto T (1990) High saturation magnetization and soft magnetic-properties of bcc Fe-Zr-B alloys with ultrafine grain-structure. *Mater Trans, JIM* 31:743–746
- [26] McHenry ME, Johnson F, Okumura H, Ohkubo T, Ramanan VRV, Laughlin DE (2003) The kinetics of nanocrystallization and microstructural observations in Finemet Nanoperm and Hitperm nanocomposite magnetic materials. *Scr Mater* 48:881–887
- [27] Highmore RJ, Greer AL (1989) Eutectics and the formation of amorphous-alloys. *Nature* 339:363–365
- [28] Cui L, Men H, Makino A et al (2009) Effect of Cu and P on the crystallization behavior of Fe-rich hetero-amorphous FeSiB alloy. *Mater Trans* 50:2515–2520
- [29] Takenaka K, Nishijima M, Makino A (2014) Effect of metalloid elements on the structures and soft magnetic properties in Fe<sub>85.2</sub>Si<sub>6.8</sub>B<sub>14-x</sub>PyCu<sub>0.8</sub> alloys. *IEEE Trans Magn* 50:2004704
- [30] Hono K, Ping DH, Ohnuma M, Onodera H (1999) Cu clustering and Si partitioning in the early crystallization stage of an Fe<sub>73.5</sub>Si<sub>13.5</sub>B<sub>9</sub>Nb<sub>3</sub>Cu<sub>1</sub> amorphous alloy. *Acta Mater* 47:997–1006
- [31] Inoue A (2000) Stabilization of metallic supercooled liquid and bulk amorphous alloys. *Acta Mater* 48:279–282
- [32] Li ZZ, Wang AD, Chang CL, Wang YG, Dong BS, Zhou SX (2014) Synthesis of FeSiBPNbCu nanocrystalline soft-magnetic alloys with high saturation magnetization. *J Alloys Compd* 611:197–200
- [33] Makino A, Men H, Kubota T, Yubuta K, Inoue A (2009) New excellent soft magnetic FeSiBPCu nanocrystallized alloys with high B-s of 1.9 T from nanohetero-amorphous phase. *IEEE Trans Magn* 45:4302–4305
- [34] Wang AD, Men H, Shen BL, Xie GQ, Makino A, Inoue A (2011) Effect of P on crystallization behavior and soft-magnetic properties of Fe<sub>83.3</sub>Si<sub>4</sub>Cu<sub>0.7</sub>B<sub>12-x</sub>P<sub>x</sub> nanocrystalline soft-magnetic alloys. *Thin Solid Films* 519:8283–8286
- [35] Ahmad Z, ul Haq A, Husain SW, Abbas T (2002) Magnetic properties of isotropic Fe–28Cr–15Co–3.5Mo permanent magnets with additives. *Phys B Condens Matter* 321:54–59
- [36] Fůzerová J, Fůzer J, Kollár P, Bureš R, Fáberová M (2013) Complex permeability and core loss of soft magnetic Fe-based nanocrystalline powder cores. *J Magn Magn Mater* 345:77–81
- [37] Dobák S, Fůzer J, Kollár P (2015) Effect of a DC transverse magnetic field on the magnetization dynamics in FeCuNbSiB ribbons and derived nanostructured powder cores. *J Alloys Compd.* 651:237–244
- [38] Chen FG, Wang YG (2014) Investigation of glass forming ability, thermal stability and soft magnetic properties of melt-spun Fe<sub>83</sub>P<sub>16-x</sub>Si<sub>x</sub>Cu<sub>1</sub> (x = 0, 1, 2, 3, 4, 5) alloy ribbons. *J Alloys Compd* 584:377–380
- [39] Jin YL, Fan XD, Men H, Liu XC, Shen BL (2012) Fe PCCu nanocrystalline alloys with excellent soft magnetic properties. *Sci China Ser E: Technol Sci* 55:3419–3424
- [40] Chen FG, Wang YG (2014) Investigation of microstructure and magnetic properties of melt spun Fe–P–C–Si–Cu ribbons. *Mater Sci Technol* 30:888–892
- [41] Patterson AL (1939) The Scherrer formula for x-ray particle size determination. *Phys Rev* 56:978–982
- [42] Kronmüller H, Fähnle M, Domann M, Grimm H, Grimm R, Gröger B (1979) Magnetic properties of amorphous ferromagnetic alloys. *J Magn Magn Mater* 13:53–70